

## Investigating the Use of Miniaturized Electrodynamic Tethers to Enhance the Capabilities of Femtosatellites and other Ultra-small Satellites

Iverson Bell and Brian Gilchrist  
*The University of Michigan*  
 Ann Arbor, Michigan 48109, USA; (734) 763-6230  
 ICBell@umich.edu

Sven G. Bilén and Jesse K. McTernan  
*The Pennsylvania State University*  
 University Park, Pennsylvania 16802, USA; (814) 863-1526  
 SBilen@engr.psu.edu

### ABSTRACT

The success of nanospacecraft and the evolution of the millimeter-scale wireless sensors concept (i.e., “SmartDust”) have generated interest in smaller spacecraft, both as stand-alone satellites and elements in a *swarm* or maneuverable *fleet*. However, so-called flat ChipSats proposed as complete spacecraft fabricated on semiconductor wafers or other larger pico- and femtosatellite, highly integrated architectures have an inherently high area-to-mass ratio, and this can result in a short orbital life in low Earth orbit (LEO) due to atmospheric drag. In this paper, we summarize trade studies in which we investigate the use of a very short (few meters), semi-rigid electrodynamic (ED) tethers for ChipSat and femtosatellite propulsion. The results reveal that an insulated tether, only a few meters long and tens of microns in diameter, can provide milligram to gram-level ChipSats with complete drag cancellation and the ability to change orbit. We build on an earlier trade study and demonstrate that the EDT system is capable of collecting sufficient current and generating the Lorentz force required for propulsion. Interestingly, the capability of maneuvering in a controlled manner represents an opportunity for any constellation of ultra-small satellites to be more of a reconfigurable, maneuverable *fleet* rather than a *swarm*.

### 1. INTRODUCTION

The burgeoning success of nanospacecraft (1-10 kg) and the evolution of the millimeter-scale wireless sensor network concept (i.e., “SmartDust”<sup>1-3</sup>) have generated interest in sensor spacecraft, either as stand-alone satellites or as elements in a *swarm* or a maneuverable *fleet*. Due to advances in integrated circuit and microelectromechanical systems (MEMS) technology, the feasibility of spacecraft at the levels of fully monolithic semiconductor integrated circuits (10 mg–1 g) or hybrid integrated circuits (1 g–1 kg) is being seriously investigated. This architecture can be thought of as a “satellite-on-a-chip” or “ChipSat”. We also refer to ChipSats as “ultra-small satellites” due to their small size. ChipSats belong to the picosatellite (100 g–1 kg) and femtosatellite (<100 g) classifications. The femtosatellite classification may be further divided into attosatellite (1-10 g) and zeptosatellite (0.1-1 g) classifications.

ChipSats can be orders of magnitude less costly to manufacture, test, and boost into orbit because of their low mass and small size.<sup>4</sup> As a result, it may be possible to launch them in large numbers, possibly enabling unique mission capabilities.<sup>5-8</sup> However, fleets of ultra-small satellites would require a high level

of coordination, and this requires maneuverability (propulsion). Flat ChipSat wafers also have an inherently high area-to-mass ratio. Although this feature can be exploited for new behaviors, it can result in a short orbital lifetime in low Earth orbit (LEO) due to atmospheric drag, ranging from a few days to a few hours depending on altitude and solar conditions.<sup>9</sup> Propulsion is needed to overcome drag.

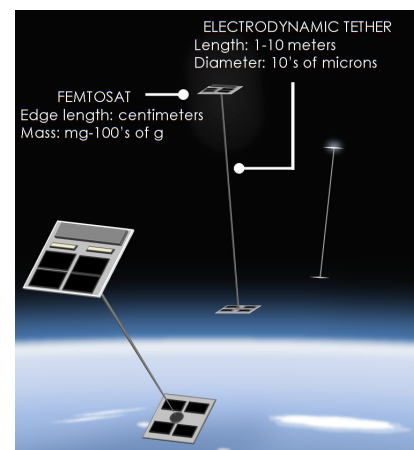


Fig. 1. Concept of ED tethers with pairs of femtosats as a maneuverable and coordinated fleet.<sup>9</sup>

In this paper, we investigate the feasibility of using a short, semi-rigid electrodynamic tether (ED tether or EDT) for propellantless propulsion. The approach appears to scale to the small size needed and provide enough thrust to overcome drag in LEO.

### 1.1. OVERVIEW OF PREVIOUS ULTRA-SMALL SATELLITE STUDIES

In this section, we describe at a high level a few ultra-small satellite designs and related studies. Barnhart, Vladimirova, and Sweeting (2006) provide a more comprehensive historical review of pico- and femtosatellite missions and designs.<sup>10</sup> Osiandor, Darrin, and Champion (2006) also provide a review, but specifically for nano- and picosatellite designs that incorporate MEMS technology.<sup>11</sup>

DARPA and the Aerospace Corporation launched a pair of picosatellites in January 2000. PicoSats 1 and 2 were identical 250 g satellites connected by a 30 meter tether.<sup>12,13</sup> Huang, Hansen, Janson, and Helvajia (2002) at the Aerospace Corporation designed and tested the structural members and key subsystems of a 100-g satellite called the Co-Orbital Satellite Assistant (COSA).<sup>14</sup> Atchinson and Peck (2009) of Cornell University designed a milligram level, 1 cm x 1 cm x 25 micron femtosatellite called "Sprite".<sup>15</sup> The Sprite ChipSat is undergoing testing on the Materials International Space Station Pallet (MISSE-8) on the International Space Station. In addition, research has been done on femtosatellite orbital evolution<sup>16</sup>, antenna design<sup>17</sup>, and radiation hardening<sup>18</sup>.

The N-prize competition has also generated interest in femtosatellites. The N-prize is a competition proposed by Dr. Paul Dear to launch a femtosatellite between 9.99 and 19.99 grams into LEO and track it for at least 9 orbits.<sup>19</sup> The competition has motivated research for a femtosatellite proof-of-concept study<sup>20</sup>, technology demonstrator<sup>21</sup>, launcher<sup>22</sup>, and payload management system<sup>23</sup>.

### 1.2. ULTRA-SMALL SATELLITE PROPULSION CONCEPTS

As described earlier, ChipSats, pico- and femtosatellites have an inherently high area-to-mass ratio, which results in an undesirably brief orbital lifetime in LEO due to atmospheric drag. Propulsion is therefore needed to increase mission lifetime. Missions using large "fleets" of satellites would also require coordination and maneuverability, again suggesting the need for propulsion. Janson and Helvajian (1999) summarize early developments of microthrusters, which are miniaturized actuators equipped with small scale micromachined nozzles and propellant reservoirs.<sup>19</sup> One microthruster propellant concept is the MEMS solid

propellant array that utilizes small, solid propellant packages that are combusted. A MEMS solid propellant microthruster array chip, for example, can lie flat, be integrated into the ChipSat structure, and provide a of thrust for each unit of propellant. A survey of MEMS-based microthrusters can be found in Rossi (2002).<sup>25</sup>

However, while a satellite using consumable propellant can overcome atmospheric drag, the volume/mass of propellant required will increase unacceptably as the desired satellite lifetime increases. The proposed Sprite spacecraft, a milligram-level, millimeter-scale architecture is capable propellantless maneuvering using the solar radiation pressure force.<sup>15</sup> Lucking, Colombo, and McInnes (2012) explore the use of an electrochromic coating on an ultra-small satellite to facilitate solar sailing.<sup>26</sup> The electrochromic coating changes reflectivity when current is passed through the material. Peck, Streetman, Saaj, and Lappas (2007) have also explored the potential to propellantlessly alter the orbit of a charged satellite as it travels through a planetary magnetic field by exploiting the Lorentz force.<sup>27</sup> This feasibility study is a continuation of previous studies in which the potential for short, semi-rigid electrodynamic tethers to provide propellantless propulsion for ultra-small satellites is investigated.<sup>9,28-30</sup>

## 2. THE MINIATURIZED ELECTRODYNAMIC TETHER PROPULSION SYSTEM CONCEPT

### 2.1. System Concept Overview

The system concept explored in this paper incorporates an insulated but conducting tether connecting a pair of nearly identical ultra-small satellites that work together as a single element. Figure 2 shows an illustration of the basic components in the concept. Each satellite is equipped with a solar panel, power supply, cold cathode electron emitter, and is capable of collecting electrons on the surface. Current conducted by the tether is collected by the satellite at one end of the tether collects electrons while the satellite at the opposite end emits electrons. Final circuit closure occurs in the ambient plasma, satisfying Kirchoff's Voltage Law. The sizes of the satellites are shown in the Table 1.

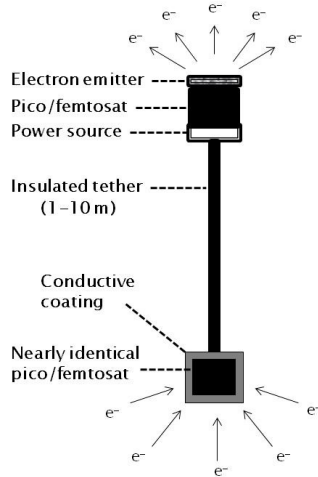


Fig. 2. A diagram showing the core components of the tether propulsion system.<sup>9</sup>

Table 1. The size, mass, and Ram area for satellites in the trade study<sup>9</sup>

Satellite Mass	Dimensions	Ram Area
400 mg	1 cm × 1 cm × 0.2 cm	0.2 cm <sup>2</sup>
2 g	1 cm × 1 cm × 1 cm	1 cm <sup>2</sup>
50 g	5 cm × 5 cm × 1 cm	5 cm <sup>2</sup>
250 g	5 cm × 5 cm × 5 cm	25 m <sup>2</sup>

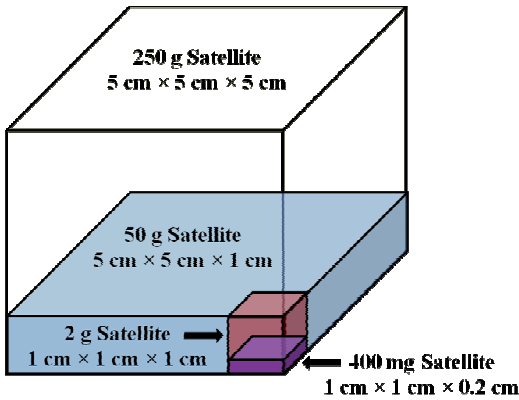


Fig. 3. The relative sizes of the femtosatellites, shown overlapping for comparison.<sup>9</sup>

## 2.2. Electrodynamic Tether Background

An electrodynamic tether is a long bare or insulated conductor connected to a spacecraft. Current traveling along the tether interacts with a planetary magnetic field to generate the Lorentz force, expressed as

$$\mathbf{F}_{\text{Lorentz}} = \int_0^L I_{\text{tether}} d\mathbf{L} \times \mathbf{B} \quad (1)$$

where  $I$  is tether current,  $d\mathbf{L}$  is a differential segment of tether with total length  $L$ , and  $\mathbf{B}$  is the magnetic field. In this paper, it is assumed that the tether conductor is insulated, straight (e.g., elongated), and perpendicular to the ambient magnetic field so the thrusting force is maximized.

The magnitude of the generated force is

$$F_{\text{Lorentz}} = I_{\text{tether}} LB \quad (2)$$

The magnitude represented by Eq. 2 can nearly be achieved at low inclination orbits for a tether that is aligned along the local vertical by the gravity gradient force. The gravity gradient force can be approximated by<sup>31</sup>

$$F_{\text{gravity-gradient}} \approx \frac{3m\mu L}{R_0^3} \quad (3)$$

where  $m$  is the total mass,  $R_0$  is the distance from the spacecraft center of mass to the Earth's center, and  $\mu$  is the standard gravitational parameter of Earth,  $3.986 \times 10^{14} \text{ m}^3 \cdot \text{s}^{-2}$ . The magnitude of the drag force is given by

$$F_{\text{drag}} = \frac{1}{2} \rho C_d A v^2 \quad (4)$$

where  $\rho$  is the neutral atmosphere density,  $A$  is the cross sectional area of the dual spacecrafts and the tether,  $v$  is the velocity of the spacecraft relative to the co-rotating atmosphere, and  $C_d$  is the drag coefficient, often assumed to be 2.2.<sup>31</sup> We assume that the tether produces force needed for drag make-up when Eq. 2 is equal to Eq. 13.

## 2.3. Tether Design Considerations

The effective length of the tether will be reduced if the tether retains residual coiling or bending from storage. To prevent this, the tether will need to be somewhat flexible. However, rigidity is needed after deployment because the gravity-gradient tension force may not straighten the tether. Thus, the tether will need to be “semi-rigid” or have a flexibility that can be changed before and after deployment.

The ED tether in this trade study has a Monel<sup>TM</sup> core to carry tether current and provide high rigidity. A thin

layer of Kapton™ provides insulation. The tether’s radius increases with length to provide a higher area moment of inertia and thus rigidity at longer lengths. The tether mass also increases with length, but this is small compared to the satellite’s masses.<sup>29</sup>

### 3. THE AMBIENT ENVIRONMENT

We consider tether propulsion at 400 km, 500 km, and 600 km altitudes in an equatorial orbit. The electron density was determined by averaging electron densities calculated at these altitudes at the equator using the International Reference Ionosphere-2007 (IRI-2007) model. This was done for January 1, 2000, which was a day with high solar activity in solar cycle 23 (F10.7D = 126). The neutral density was similarly taken from the Mass-Spectrometer-Incoherent-Scatter (MSIS-E-90) model. Atmosphere and ionosphere assumptions are summarized in table 2. The assumed spacecraft velocity relative to the Earth’s co-rotating atmosphere is  $7.5 \text{ km}\cdot\text{s}^{-1}$ .

Table 2. Ionospheric and atmospheric conditions

Parameter	400 km Altitude	500 km Altitude	600 km Altitude
Electron Temp.	0.11 eV	0.14 eV	0.15 eV
Magnetic Field	0.3 gauss	0.3 gauss	0.3 gauss
Gyroradius	3 cm	3 cm	3 cm
Neutral Density	$5\times 10^{-15} \text{ g}\cdot\text{cm}^{-3}$	$9\times 10^{-16} \text{ g}\cdot\text{cm}^{-3}$	$2\times 10^{-16} \text{ g}\cdot\text{cm}^{-3}$
Electron Density	$1\times 10^6 \text{ electrons}\cdot\text{cm}^{-3}$	$7\times 10^5 \text{ electrons}\cdot\text{cm}^{-3}$	$3\times 10^5 \text{ electrons}\cdot\text{cm}^{-3}$
Debye Length	2 mm	3 mm	5 mm
Electron-to-neutral Density	$5\times 10^{20} \text{ electrons}\cdot\text{g}^{-1}$	$5\times 10^{20} \text{ electrons}\cdot\text{g}^{-1}$	$5\times 10^{20} \text{ electrons}\cdot\text{g}^{-1}$

### 4. ELECTRON COLLECTION

Estimating the electron collection current to the surfaces of a biased pico- or femtosatellite is a complex problem. A variety of simplifying assumptions have been made here to facilitate estimating this current. However, an experiment that captures the critical characteristics of the ultra-small satellites’ interaction with the LEO environment will be needed in order to provide a more accurate current collection estimate.

Following the “spherical collector” assumption, we estimate current collection by assuming that the anode collects current like a sphere with an equivalent diameter equal to the satellite’s longest edge. The equivalent radii of the 400 mg and 2 g satellites are 5 mm while the equivalent radii of the 50 g and 250 g satellites are 2.5 cm.

#### 4.1. The spherical collector approximation for electron collection

A positively biased conductor immersed in plasma will generate an electric field that attracts electrons from the plasma and causes the formation of a non-neutral sheath region between the immersed object’s surface and the ambient plasma. Here, we assume that there is no emitted current that escapes from the sheath (e.g. no ion production and no secondary photo-electrons that can escape). From a practical standpoint, therefore, the current in the tether and collected to the probe current must equal the net current passing through the outer edge of the sheath boundary. Here, we also assume that the potential difference between the probe and the undisturbed ambient plasma is much larger than the electron temperature,  $T_e$ , and falls exclusively across the sheath. This ignores a small fraction of the potential, on the order of the electron temperature, that falls across an extended pre-sheath region.<sup>32</sup>

Finally, we assume that the tether current can be collected on any of the pico- or femtosatellite outer surface. To facilitate electron collection, areas of the satellite’s outer surface can be coated with a transparent conductor, e.g., Indium Tin Oxide (ITO).

Estimating the current that the satellite can collect at a given potential is a complex problem. Current collection models provide relationship between the anode bias and the plasma potential for less complex geometries like spheres, infinite cylinders, and infinite plates. The satellites, however, are cuboids and this complicates estimating collection current. The authors are not aware of any experiments in LEO that studied current collection to similar structures of the same scale in typical ionospheric conditions.

In this paper, we reason that the satellites’ potentials ( $V_{\text{anode}}$ ) will need to be large with respect to the ambient electron temperature ( $T_e$ ) expressed in terms of volts to collect the needed drag make-up current from the ionosphere, and this results in the formation of a sheath. At this large potential, we assume the sheath is much larger than the Debye length, which is

$$\lambda_D = \sqrt{\frac{\epsilon_0 T_e}{qn_e}} \quad (5)$$

where  $T_e$  is electron temperature,  $n_e$  is electron density,  $q$  is  $1.6\times 10^{-19} \text{ C}$ , and  $\epsilon_0$  is  $8.85\times 10^{-12} \text{ F}\cdot\text{m}^{-1}$ .

Here, we estimate the sheath size. Given a spherical probe where  $V_{\text{anode}} > \Phi_p$  (e.g., the electron saturation regime), if the probe dimension is small with respect to  $\lambda_D$  and the plasma is collisionless, non-drifting,

unmagnetized, and Maxwellian, the collection current is given by<sup>33</sup>

$$I_{OML} = I_{\text{thermal}} \left( 1 + \frac{q(V_{\text{anode}} - \Phi_p)}{kT_e} \right), \quad (6)$$

where  $kT_e/q$  is the electron temperature in eV and the thermal current  $I_{\text{thermal}}$  is

$$I_{\text{thermal}} = A_{\text{probe}} n_e q \sqrt{\frac{kT_e}{2\pi m_e}}. \quad (7)$$

Equation (6) gives us the Orbit Motion Limited (OML) current, which is the collection current characteristic if the sheath is large or “thick” relative to the probe size. Eq. (7) gives us the collection current if the sheath is very small or “thin” relative to the probe size. Following the assumptions of OML theory, the sheath edge should collect thermal current (disregarding the small potential in the pre-sheath) and accelerate these electrons to the probe. The sheath current is simply the product of the sheath surface area ( $4\pi r_{\text{sheath}}^2$ ) and the thermal current density. Since the current at the sheath edge is equal to the current collected by the probe, we can solve for a rough approximation of the sheath radius, given as

$$r_{\text{sheath}} = r_{\text{probe}} \sqrt{1 + \frac{q(V_{\text{probe}} - \phi_p)}{kT_e}}. \quad (8)$$

For a sphere in a 0.1 eV temperature plasma charged to 10 volts above the plasma potential, the sheath radius is approximately 10 times the probe radius while a sphere charged to 100 V has an estimated sheath radius around 30 times the probe radius. The large approximate estimated sheath size helps justify using the spherical collector approximation. Sheridan (2010) shows the expansion of an ion collecting sheath in a stationary plasma with sheath radius increasing with potential, where at high potentials the sheath resembles an oblate spheroid.<sup>34</sup>

#### 4.2. Picking a model to estimate collection current

The complex LEO environment also creates a current collection scenario that no analytical model the authors are aware of completely captures in our size scale. The orbital motion of the satellite relative to the ionosphere violates the isotropic Maxwellian plasma assumption of the OML theory. Satellites in LEO travel faster than the ion thermal speed and slower than the electron thermal speed, or at mesosonic speed.<sup>35</sup> The high speed flowing

plasma has a beam-like effect and creates a wake region behind the probe.

OML theory also does not apply because the plasma in LEO is weakly magnetized. Disregarding collisions and electric fields, electrons in LEO travel along magnetic flux tubes. The electron gyroradius is

$$r_L = \frac{m_e v_{\perp}}{eB} \quad (9)$$

where  $B$  is the magnetic field strength and  $v_{\perp}$  is the component of electron velocity perpendicular to the magnetic field. The model for electron collection by a biased sphere in non-flowing, magnetized plasma is provided by Parker-Murphy as<sup>36</sup>

$$I_{PM} = \frac{I_{\text{thermal}}}{2} \left( 1 + \left( \frac{V_{\text{anode}} - \phi_p}{\phi_o} \right)^{1/2} \right) \quad (10)$$

where the intermediate potential  $\phi_o$  is given by

$$\phi_o = \frac{m_e \omega_{ce}^2 r_{\text{sat}}^2}{8q}. \quad (11)$$

The thermal current in Eq. (10) is divided by 2 because the collection area is  $2\pi r^2$ , or the 2-dimensional projection area of the front and back of a sphere. The current collected by the sphere is limited to only the electrons trapped on intersecting flux tubes and as a result the Parker Murphy current is less than the OML current when  $V_{\text{anode}} \gg \Phi_p$ .

The Parker-Murphy model was modified by mission data from the Tether Satellite Systems Reflight (TSS-1R) to account for mesothermal plasma speed, giving the expression<sup>37</sup>

$$I_{\text{TSS-1R}} = \alpha \frac{I_{\text{thermal}}}{2} \left( 1 + \left( \frac{V_{\text{anode}} - \phi_p}{\phi_o} \right)^{\beta} \right) \quad (12)$$

where  $\beta \approx 0.5$  and  $\alpha \approx 2.5$ . One of the assumptions of the Park-Murphy model and the TSS-1R modified Parker-Murphy model is that the gyroradius is small with respect to the collector size. The average electron gyroradius is approximately 3 cm in the region of LEO we are considering in the trade study. The TSS-1R anode had a radius of 0.8 m while the largest satellite in this trade study has an equivalent radius of 2.5 cm. Thus the TSS-1R modified Parker-Murphy model does

not capture the effect of the small size of the satellite with respect to the gyroradius.

Alternatively, Barjatya, Swenson, Thompson, and Wright (2007) provide a strategy for extracting plasma parameters from empirical current collection measurements in LEO. Although it is imprecise, we reverse their strategy and use the plasma parameters to estimate the collected current. The wide-sweeping Langmuir probe (WLP) instrument is a 5 cm radius gold spherical probe located on the International Space Station. The WLP is only slightly larger than the 250 g and 50 g satellites and reaches voltages as high as 80 V, which is higher than many Langmuir probes in LEO and is also more similar to the anode voltages reached by the 50 and 250 g satellites. The expression<sup>38</sup>

$$I_{WLP} = \frac{I_{\text{thermal}}}{2} \left( 1 + \frac{q(V_{\text{anode}} - \Phi_p)}{kT_e} \right)^\beta \quad (13)$$

was fit to WLP current-voltage sweeps with varying values of the dimensionless parameter  $\beta$ . The resulting electron density and temperature measurements derived from this method appear to match measurements from other instruments in the suite. Similar to the Parker-Murphy model, the term  $I_{\text{thermal}}/2$  represents the 2-dimensional projection area of the front and back of a sphere

When  $\beta = 1$ , the current is in the OML regime. Changing the value of  $\beta$  to  $1/2$  reduces the current to that of a collecting cylinder, which is less and also closer to the Parker-Murphy value. In a single several-hour time window shown in Barjatya *et al.* (2007), the values of  $\beta$  vary between 0.5 and 1, with an average approximately of 0.8.<sup>38</sup> We expect the ChipSat collected current to fall below the OML current and above the Parker-Murphy current, so we conservatively choose  $\beta = 0.85$  for our model, which satisfies this condition and is close to the apparently average  $\beta$  value observed in the time window in Barjatya *et al.* (2007).

## 5. ELECTRON EMISSION

A field emitter array (FEA) can be used to emit electrons at the opposite end of the tether. The emitting structure can be fabricated using submicron-scale sharp tipped cones, like the ‘‘Sphindt Cathode’’, or nanorods. A positive bias  $V_{\text{gate}}$  can be applied to a gate near the emitting surface, generating an intense electric field that lowers the effective work function of the emitting material and facilitates electron emission and acceleration across the gap. Large numbers of tips can be arranged to produce a beam of electron current. The electron current used in this trade study is a version of the Fowler-Nordheim emission law, given as<sup>39</sup>

$$I_{\text{cathode}} = a_{\text{FN}} V_{\text{gate}}^2 \exp(-b_{\text{FN}}/V_{\text{gate}}) . \quad (14)$$

We chose to use a 1-mm diameter Sphindt Cathode FEA emitter for this trade study. The values used for Fowler-Nordheim coefficient in Eq. 14 are  $a_{\text{FN}} = 0.03 \text{ A}\cdot\text{V}^{-2}$  and  $b_{\text{FN}} = 487 \text{ V}$ .

The electrons emitted from the FEA can create a potential barrier for additional emitted electrons. There is a maximum space charge limited current density that can be achieved at a given bias. The potential impact of the space charge limited current density on the design was explored in Bell (2012).<sup>9</sup>

## 6. POWER

### 6.1. Estimating Thrust Power

The ED tether requires on-board electrical power to generate thrust to add energy to the orbit. The total power needed for propulsion ( $P_{\text{thrust}}$ ) is the sum of the electrical power dissipated in the tether  $|I_{\text{tether}}|^2 R$ , the anode  $|I_{\text{tether}} V_{\text{anode}}|$ , and the cathode  $|I_{\text{tether}} V_{\text{gate}}|$  (It is assumed that potential from spacecraft to the ambient Ionospheric plasma on the cathode tether end is negligible) as well as the power required to overcome the electromotive force  $|I_{\text{tether}} V_{\text{emf}}|$ . We are assuming that the impedance of the plasma and the voltage drop across the sheath traversed by electrons emitted from the cathode is negligible. For this short tether application, as we will see, the power required by the anode and cathode make up a majority of the electrical demand. Additional inefficiencies in power generation and distribution are considered later in this section.

To estimate the minimum current needed for drag make-up, the assumed ED thrust (Eq. 2) is set equal to the drag force (Eq. 4), giving the tether current needed for drag make-up,

$$I_{\text{tether}} = \frac{1/2 \rho C_d A v^2}{LB} . \quad (15)$$

The needed tether current is dependent on neutral density, so if the neutral density increases due to a change in ambient conditions, the drag make-up current must increase as well.

For a tether oriented along the local vertical in a low inclination orbit, the electromotive force (EMF) can be approximated as

$$V_{\text{emf}} = vLB \quad (16)$$

The EMF is naturally induced along the tether in the presence of the magnetic field. The current resulting

from the EMF in prograde orbits de-orbits a satellite, so the power supply voltage must exceed the EMF and be of opposite polarity to produce boost. The electromotive force is small for tethers of this scale.

The power dissipated in the tether is not a dominant factor because this loss term scales with resistance and the square of current, both of which are small values.<sup>30</sup> The tether resistance is given by

$$R = \rho_{\text{resistivity}} \left( \frac{L}{A} \right). \quad (17)$$

The anode and cathode gate voltages can be derived by rearranging equations (13) and (14), respectively. The cathode potential is

$$V_{\text{gate}} = \frac{b_{FN}}{2W \left( b_{FN} \sqrt{\frac{a_{FN}}{I_{\text{tether}}}} \right)} \quad (18)$$

where  $W$  is the Lambert  $W$  function. The anode potential is

$$V_{\text{anode}} = \phi_p + \frac{kT_e}{q} \left( \left( \frac{I_{\text{tether}}}{I_{\text{thermal}}} \right)^{1/\beta} - 1 \right). \quad (19)$$

## 6.2. Estimating Power Available for Propulsion

Photovoltaic (PV) cells or solar cells lining the outer surface of the pico- or femtosatellite can generate long-term power. PV cells generate electrical power when illuminated by sunlight. Ideal solar cell output per unit area in LEO would be  $1368 \text{ W}\cdot\text{m}^{-2}$  or  $136.8 \text{ mW}\cdot\text{cm}^{-2}$ . However, PV cells have an energy conversion efficiency ( $\eta_{\text{conversion}}$ ), so only a portion of the received solar power is converted into DC power for the satellite and propulsion system.

Small, off-the-shelf photovoltaic cell have efficiencies exceeding 15%, but they cannot be monolithically integrated into CMOS fabricated ChipSats because the fabrication processes for CMOS and the commonly used PV cells are incompatible.<sup>10</sup> While larger ChipSats may be able to utilize higher efficiency solar cells though hybrid assembly, it is possible that the smallest ChipSat architectures may primarily be monolithic. The silicon-on-insulator (SOI) fabrication process, however, has demonstrated monolithic integration of PV cells in CMOS and MEMS with energy conversion efficiencies above 11%.<sup>3</sup> We conservatively estimate that the solar cells have an

energy conversion efficiency of 10%, or an output performance per unit area of  $13.7 \text{ mW}\cdot\text{cm}^{-2}$ . It may also be possible to integrate a maximum power point circuit to extract the maximum power from the solar cells, as was done in the satellite design in Barnhart, Vladimirova, Baker and Sweeting (2009).<sup>4</sup>

The received power is proportional to the cosine of the solar angle of incidence, which is the angle between the incident light and the surface normal. We assume an average solar angle of  $45^\circ$ . The resulting estimated output power per unit area provided by the solar cells is  $9.7 \text{ mW}\cdot\text{cm}^{-2}$ . Lifetime degradation is not considered in this feasibility study.

For this iteration of the trade study, we assume that ED thrust power will be needed continuously throughout the orbit. Atmospheric drag can de-orbit the smallest ChipSats rapidly, as shown in Reference 9, so it may be important for the tether to provide thrust during the day and eclipse. No power is provided to the solar cells during eclipse, however, so some portion of the solar cell output power will be used for thrusting during the day while another portion is stored for thrusting during eclipse. The remainder is dissipated or used by other loads.

To estimate the peak thrusting capability of the ED tether, we assume that the power available for propulsion ( $P_{\text{available}}$ ) is 90% of the power requirements during daylight ( $P_d$ ) and eclipse ( $P_{\text{ecl}}$ ), or  $0.9 \cdot P_{\text{available}} = (P_{\text{ecl}} + P_d)$ . At 400 km, eclipse is approximately 36 minutes and the orbital period is approximately 92 minutes, so the fraction of the orbital period in eclipse ( $T_{\text{ecl}}$ ) is roughly 0.4.<sup>31</sup> Values of  $T_{\text{ecl}}$  at 500 km and 600 km altitudes are similar. We also assume that 15% of the overall solar array output will be lost in a step-up voltage DC-DC converter and other loads during daylight and eclipse, so the fraction of generated power available the propulsion system during the day ( $X_d$ ) and eclipse ( $X_e$ ) is 0.85. The solar array power output per unit area can be expressed as<sup>31</sup>

$$P_{\text{sa}} = \frac{\left( \left( \frac{P_{\text{ecl}} T_{\text{ecl}}}{X_{\text{ecl}}} \right) + \left( \frac{P_d T_d}{X_d} \right) \right)}{T_d}. \quad (20)$$

Using Eq. (20), we can estimate the electrical power available for ED thrusting per unit area. We find that roughly  $4.5 \text{ mW}\cdot\text{cm}^{-2}$  are available for propulsion, which is about 3% of the total incident radiated power per unit area. An estimate of the total generated power available for propulsion can be found by multiplying  $4.5 \text{ mW}\cdot\text{cm}^{-2}$  by the PV area. We assume the ChipSats have solar panels on all six sides of the upper and lower

end-bodies, three of which are exposed to the sun at any given time.

### 6.3. Comparing Estimated Power Needed for Propulsion to the Estimated Power Available for Propulsion

Figures 4a-d show estimated power required for drag make-up at 400 km (black), 500 km (green), and 600 km (blue). The red dashed line in the figures represents the available thrust power. If the power required for drag make-up exceeds the available thrust power, the EDT cannot overcome the drag force. However, if the converse is true and the pico- or femtosatellite has more power available than is required for thrust, the EDT can boost.

The shape of the power-length curve also suggests that there may be an optimal tether length. Short ED tether lengths are preferable, but they require a large current to overcome the drag force on the satellite. The rigidity of a tether decreases with length, so a very long EDT must have a relatively large radius to prevent bowing. As a result, the drag due to the tether dominates over the drag due to the satellite, driving up the required current. The current is minimized when these two effects are balanced. This motivates us to choose a 1 m, 4 m, 5 m, and 12 m long tether for the 400 mg, 2 g, 50 g, and 250 g satellites, respectively.

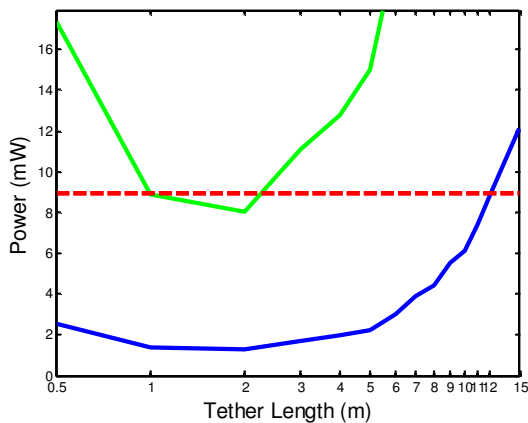


Figure 4a. Estimated power needed for drag make-up at 400 km (not shown), 500 km (green), and 600 km (blue) and power available for propulsion (red, 9 mW) for the 400 mg satellite.

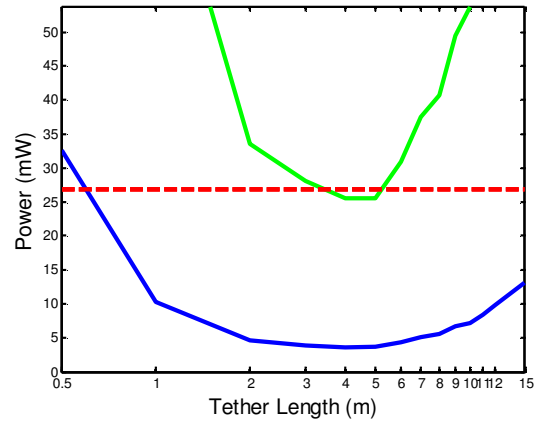


Figure 4b. Estimated power needed for drag make-up at 400 km (not shown), 500 km (green), and 600 km (blue) and power available for propulsion (red, 27 mW) for the 2 g satellite.

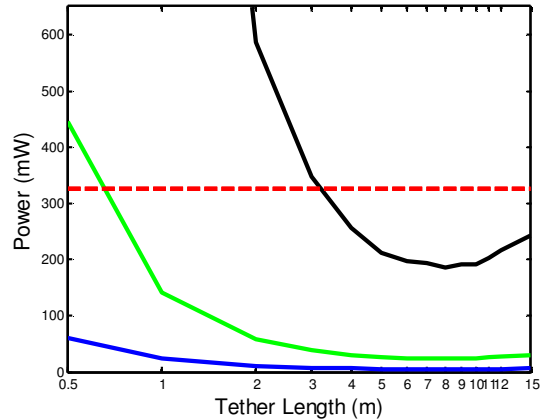


Figure 4c. Estimated power needed for drag make-up at 400 km (black), 500 km (green), and 600 km (blue) and power available for propulsion (red, 318 mW) for the 50 g satellite.

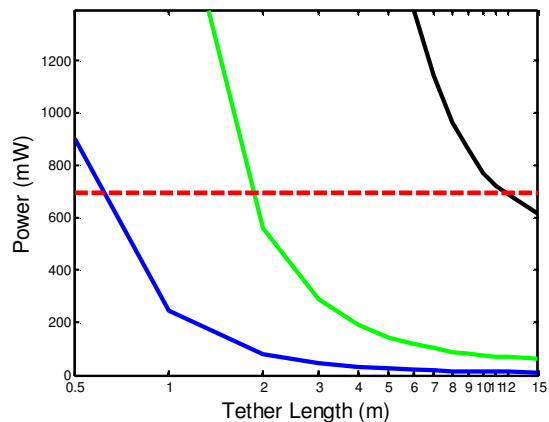


Figure 4d. Estimated power needed for drag make-up at 400 km (black), 500 km (green), and 600 km (blue) and power available for propulsion (red, 672 mW) for the 250 g satellite.

#### 6.4. ED Tether Power Generation for Nanosatellites

An electrodynamic tether can also generate power. Bilén *et al.* (2010) explores the potential for a 10 cm × 10 cm × 30 cm nanosatellite, or “3U CubeSat”, with a starting altitude of 500 km (circular) and a 28° inclination.<sup>40</sup> Simulations done by Bilén *et al.* (2010) show that a 1300 m aluminum tether stored in a single 10 cm × 10 cm × 10 cm unit of the nanosatellite is capable of producing around 44 W peak power and 42 W average power over a 10 minute period.<sup>40</sup> However, a satellite equipped with an EDT harvesting system will lose altitude while in harvesting mode. This is due to a Lorentz force interaction between the current flowing in the tether and the geomagnetic field.

Power generation is significantly limited by the ability of plasma contactors to facilitate current flow between the spacecraft and the surrounding plasma environment. Relatively small satellites are further limited by mass and volume constraints. Therefore, effective power generation for ultra-small spacecraft will require advances in plasma contactor technology that produces compact and efficient contactors.

#### 7. ESTIMATING THE DOMINANT FORCES ON THE SYSTEM

The drag, gravity gradient force, and radiation pressure forces are the dominant forces for a satellite orbiting in the altitudes considered for this trade study.<sup>41</sup> We use Eq. (3) to estimate the gravity gradient force, Eq. (4) to estimate the drag force, and Eq. (2) to estimate the maximum tether thrust. To estimate the solar radiation pressure force, we calculate the force on 2 sides of each end-body as<sup>42</sup>

$$F_{\text{plate}} = \frac{2A\Phi_{\text{direct}}}{3c} \sin \theta \left[ \frac{(3 + \Gamma_{\text{spec}})}{\pi} \sin \theta + \frac{\Gamma_{\text{diffuse}}}{2} \right] \quad (15)$$

and the lateral force on the tether as<sup>42</sup>

$$F_{\text{cyl}} = \frac{2\pi r_i L \Phi_{\text{direct}}}{3c} \sin \theta \left[ \frac{(3 + \Gamma_{\text{spec}})}{\pi} \sin \theta + \frac{\Gamma_{\text{diffuse}}}{2} \right] \quad (16)$$

where  $c$  is the speed of light,  $A$  is the RAM area of both satellites,  $\Phi_{\text{direct}}$  is the direct solar radiation flux,  $\Gamma_{\text{diffuse}}$  is the diffuse coefficient of reflectivity, and  $\Gamma_{\text{spec}}$  is the specular coefficient of reflectivity. These values are provided in Bell (2011).<sup>30</sup> We assume that on average the light reflects off surface at  $\theta = 45^\circ$ . For our solar pressure estimate, we assume that the total force is simply the sum of Eqs. 15 and 16.

Figures 5a-d show an estimate of the dominant forces at a 400 km, 500 km, and 600 km altitude. All four of the satellites are able to provide thrust equivalent to drag at 500 km and 600 km. The neutral density increases at 400 km, however, and only the satellites with more power available to provide the necessary drag make-up thrust are able to boost at this altitude. The solar radiation pressure force is below other forces for all the satellites. The gravity gradient force decreases with increasing altitude, but the variation from 400 km to 600 km is very small so only one gravity gradient curve is shown for each satellite. The gravity gradient force is included because a strong gravity gradient force suggests a restoring torque may provide satellite attitude stability.

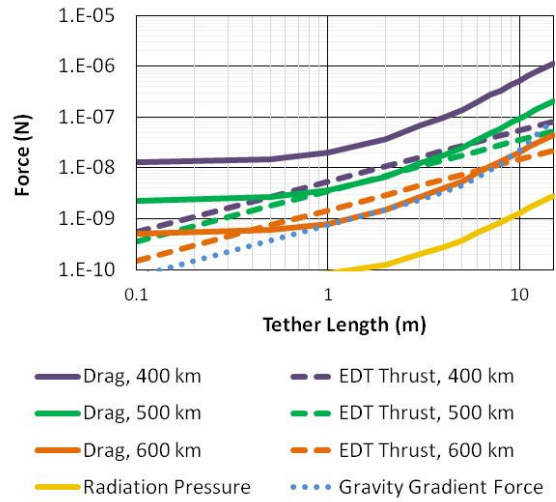


Fig. 5a. Estimate of the dominant forces on the dual 400 mg satellite and EDT system at 400 km, 500 km, and 600 km.

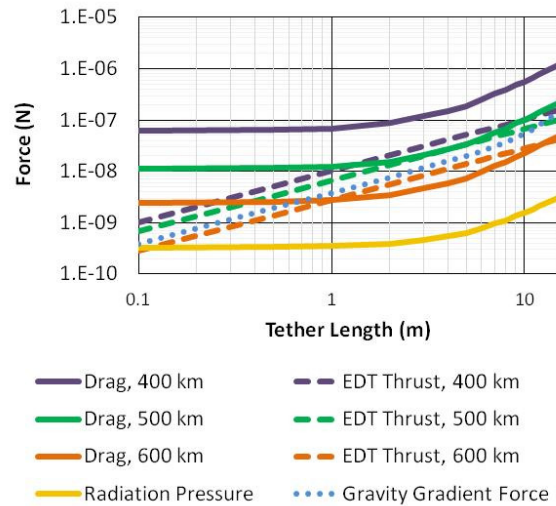


Fig. 5b. Estimate of the dominant forces on the dual 2 g satellite and EDT system at 400 km, 500 km, and 600 km.

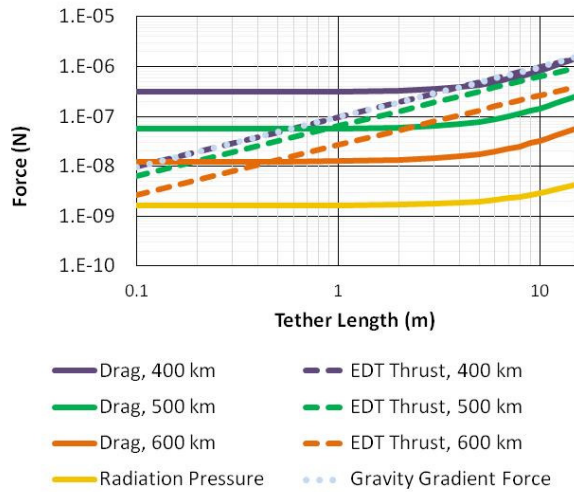


Fig. 5c. Estimate of the dominant forces on the dual 50 g satellite and EDT system at 400 km, 500 km, and 600 km.

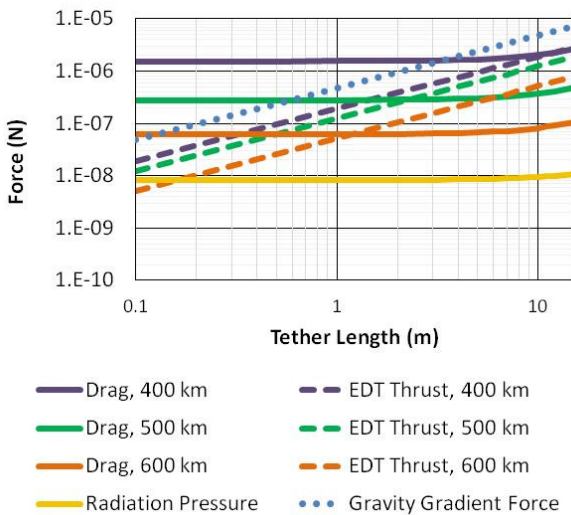


Fig. 5d. Estimate of the dominant forces on the dual 250 g satellite and EDT system at 400 km, 500 km, and 600 km.

The ED tethers used for pico- and femtosatellite propulsion are miniaturized to the scale of these small satellites, but this has the unfortunate effect of reducing the gravity gradient force. To understand how the gravity gradient force reduces with tether size, we assess how it scales with tether length. The radius of miniaturized ED tethers ( $r_t$ ) increases with length ( $L$ ), so  $r_t$  is proportional to  $L$ . Likewise, the tether volume ( $\pi r_t^2 L$ ) and mass are proportional to  $L^3$ . As a result, the gravity gradient force, which scales with mass and length, is proportional to  $L^4$ . The drag force, on the other hand, is proportional to the total ram area, which we assume is simply the sum of the satellite ram area and the tether ram area ( $2r_t L$ ). The tether radius  $r_t$  is

proportional to  $L$ , so the total area and the resulting drag force roughly scale with  $\sim L^2$ . Therefore, miniaturizing the tether causes the gravity gradient force to decrease much more rapidly than the drag force, and this challenges our assumption that the gravity gradient force and torque ensure gravity gradient stability.

The low mass of the end-bodies also contributes to the gravity gradient force being small. The larger satellites (50 g and 250 g) generate a gravity gradient on the order of the drag force at 400 km, 500 km, and 600 km. For the smallest satellites (400 mg and 2 g), however, the gravity gradient force is smaller and on par with drag at 600 km but is exceeded at lower altitudes. It may be necessary to consider other architectures of deployed tethers that can address both drag and attitude control.<sup>43</sup> However, this is beyond the scope of the current paper.

## 8. CONCLUSION

This paper shows that an ED tether scales to the small size needed, is propellantless, keeps the overall ChipSat mass low, and is able to overcome drag in LEO. The system concept is summarized below. The results of this research will guide optimal system configurations and reveal new capabilities for utilizing ED tethers with pico- and femtosatellite technology. Many of these approximations are very conservative and future research will allow us to estimate performance more precisely.

Table 3. System concept summary

Parameter	400 mg	2 g	50 g	250 g
Satellite Dimensions	1 cm × 1 cm × 0.2 cm	1 cm × 1 cm × 1 cm	5 cm × 5 cm × 1 cm	5 cm × 5 cm × 5 cm
Tether	1 m long, 24 μm diam.	4 m long, 70 μm diam.	5 m long, 80 μm diam.	1 m long, 200 μm diam.
Mass	2 mg	12 mg	0.18 g	3 g
Thrust Power	9 mW	27 mW	318 mW	672 mW
Where is gravity gradient significant?	~600 km	~500 km, 600 km	~400 km, 500 km, 600 km	400 km, 500 km, 600 km

### Acknowledgments

The authors gratefully acknowledge support from AFOSR grant FA9550-09-1-0646 and the National Science Foundation.

## References

1. Kahn, J. M., Katz, R. H., and Pister, K. S. J., "Next Century
2. Challenges: Mobile Networking for Smart Dust," *Proc. ACM MobiCom '99*, Washington, DC, 1999, pp. 271–78.
3. Warneke, B.A., et al., "An Autonomous 16 mm<sup>3</sup> Solar-powered Node for Distributed Wireless Sensor Networks," *IEEE Sensors 2002 Proceedings*, Vol. 2, p. 1510–1515, 2002.
4. Barnhart, D.J., Vladimirova, T., Baker, M. and Sweeting, M. N., "A Low-cost Femtosatellite to Enable Distributed Space Missions," *Acta Astronautica* (June 2009), pp. 1123-1143.
5. Barnhart, D.J., Vladimirova, T., and Sweeting, M., "Very-small-satellite Design for Distributed Space Missions," *Journal of Spacecraft and Rockets*, Vol. 44, No. 6, 2007, pp. 1294–1306.
6. Balthazor, R.L., McHarg, M.G., Godbold, C.S., Barnhart, D.J., Vladimirova, T., "Distributed Space-based Ionospheric Multiple Plasma Sensor Networks" in Aerospace Conference, 2009 IEEE, Big Sky, MT 2009.
7. Sundaramoorthy, P.P., Gill, E.K.A., Verhoeven, C.J.M., "Systematic Identification of Applications for a Cluster of Femto-Satellites," 61st International Astronautical Congress, Prague, CZ, 2010.
8. J. Bouwmeester, J. Guo, "Survey of Worldwide Pico- and Nanosatellite Missions, Distributions and Subsystem Technology," *Acta Astronautica* Vol. 67, Netherlands, 2010.
9. Bell, I., Liaw, D., Gilchrist, B., McTernan, J., Bilén, S., Voronka, N., Hoyt, R., Peck, M., "Electrodynamic Tethers for ChipSat and Nanospacecrafts," *Spacecraft Charging and Technology Conference*, Kitakyushu, Japan, May 15 2012.
10. Barnhart, D.J., Vladimirova, T., and Sweeting, M., "Satellite-on-a-chip development for future distributed space missions," in *Proceedings of the CANEUS Conference on Micro–Nano Technologies for Aerospace Applications*, Toulouse, France, 2006 (Paper CANEUS2006-11045).
11. Osiandor, R, Darrin, M.A.G, Champion, J. L., Ed., "MEMS and Microstructures in Aerospace Applications," Boca Raton, FL: CRC 2006.
12. Tang, W. C., "Overview of MEMS Programs at DARPA and Applications in Space," Presentation, First Canadian Workshop on MEMS Technology for Aerospace Applications, National Research Council, Canada, April 12, 2001.
13. Hinkley, D., "Picosatellites at The Aerospace Corporation," Chapter 20 in *Small Satellites: Past, Present, and Future*, edited by H. Helvajian and S. W. Janson (The Aerospace Press and the AIAA, El Segundo, CA, 2009).
14. Huang, A., Hansen, W.W., Janson, S.W., Helvajian, H., "Development of a 100-gm-class Inspector Satellite Using Photostructurable Glass/ceramic Materials" *Proc. SPIE 4559*, 164 (2001).
15. Atchison, J. A. and Peck, M. A., "A Passive, Sun-Pointing, Millimeter-Scale Solar Sail," *Acta Astronautica*, Vol. 67, No. 1-2, 2009, pp. 108-121.
16. Colombo, C. Lucking, C. and McInnes, C.mR., "Orbit evolution, maintenance and disposal of SpaceChip swarms". in 6th International Workshop on Satellite Constellation and Formation Flying, Taipei, Taiwan, 2010.
17. Fernandez-Murcia, E., Izquierdo, L., and Tristanchó, J. "A synthetic aperture antenna for femto-satellites based on commercial-of-the-shelf" 2011 IEEE/AIAA 30th Digital Avionics Systems Conference, Seattle, WA, 2011.
18. Barnhart, D. J., Vladimirova, T., Sweeting, M. N., "Design of Self-Powered Wireless System on-a-Chip Sensor Nodes for Hostile Environments," in *Proc. IEEE International Symp. On Circuits and Systems*, Seattle, WA, 2008, Paper 1869.
19. Dear, P. H. N-prize, rules in full. [http://www.n-prize.com/assets/rules\\_in\\_full.pdf](http://www.n-prize.com/assets/rules_in_full.pdf), 2008.
20. Tristanchó, J. and Gutierrez-Cabello, J. "A Probe of Concept of Femto-Satellite Based on Commercial Off-The-Shelf," 29th Digital Avionics Systems Conference, Seattle, 2011.
21. Kravchenko, V., "Design and Implementation of a Femto-satellite Technology Demonstrator," *Universitat Politecnica de Catalunya Master Thesis*, 2011.
22. Tristanchó, J., "Implementation of a femto-satellite and a mini-launcher for the N Prize", *Universitat Politecnica de Catalunya Master Thesis*, 2010.
23. Navarro Morales, L., "A Multi-agent Payload Management Approach for Femtosatellite Applications," *Universitat Politecnica de Catalunya Master Thesis*, 2011.

24. Janson, W. and Helvajian, H. "MEMS, Microengineering and Aerospace Systems," AIAA Paper 99-3802, 1999.
25. Rossi, C., "Micropropulsion for Space — A Survey of MEMS-based Micro Thrusters and their Solid Propellant Technology," *Sensors Update*, 10: 257–292, 2002.
26. Lucking, C., Colombo, C., and McInnes, C. "Electrochromic orbit control for smart-dust devices," *Journal of Guidance, Control and Dynamics*, 2012.
27. Peck, M. A., Streetman, B., Saaj, C. M., and Lappas, V., "Spacecraft Formation Flying Using Lorentz Forces," *Journal of the British Interplanetary Society*, Vol. 60, July 2007, pp. 263–267.
28. Bell, I.C., "Electrodynamic Tethers for ChipSat and Nanospacecrafts." Poster, *Spacecraft Charging and Technology Conference*, Albuquerque, NM, Sept 23 2010.
29. Bell, I., Gilchrist, B., McTernan, J., Bilén, S., Voronka, N., Hoyt, R., Peck, M., "The Potential of Miniature Electrodynamic Tethers to Enhance Capabilities of Femtosatellites," IEPC-2011-054, 32nd International Electric Propulsion Conference, Wiesbaden, Germany, 15 Sept. 2011.
30. Bell, I., Gilchrist, B., McTernan, J., Bilén, S., Voronka, N., Hoyt, R., Peck, M., "Enabling Ultra-small Sensor Spacecraft for the Space Environment using Small-Scale Electrodynamic Tethers." AIAA SPACE 2011 Conference and Exposition, Long Beach, California, Sep. 27-29, 2011, AIAA-2011-7322.
31. Wertz, J.R., Everett, F.D., and Puschell, J.J. (eds.), *Space Mission Analysis and Design*, Microcosm, Inc., 2011.
32. Lieberman, M. A., and Lichtenberg, A. J., *Principles of Plasma Discharges and Materials Processing*. Wiley and Sons, New York, 2005.
33. Mott-Smith, H.M. and Langmuir, I. "The Theory of Collectors in Gaseous Discharges," *Phys. Rev.*, Vol. 28, pp. 727–763, 1926.
34. Sheridan, T.E. "How big is a small Langmuir probe" *Phys. Plasmas* 7, 3084, 2000.
35. Fuhrhop, K.R.P., "Theory and Experimental Evaluation of Electrodynamic Tether Systems and Related Technologies." Ph.D. Thesis, The University of Michigan, pp. 1–53, 2007.
36. Parker, L W., and Murphy, B.L., "Potential Buildup on an Electron Emitting Ionospheric Satellite," *J. Geophys. Res.*, Vol. 72, p. 1631, 1967.
37. Thompson, D.C., Bonifazi, C., Gilchrist, B.E., "The current-voltage characteristics of a large probe in low Earth orbit: TSS-1R results," *Geophysical Research Letters*, Vol. 25, No. 4, 1998, pp. 413-416.
38. A. Barjatya, C. M. Swenson, D. C. Thompson, and K. H. Wright, Jr., "Data analysis of the floating potential measurement unit aboard the international space station," *Rev. Sci. Instrum.*, 2008.
39. Whaley, D., *et al.*, "100 W Operation of a Cold Cathode TWT," *IEEE Trans. Electron Devices*, Vol. 56, No. 5, pp. 896–905, May 2009.
40. Bilen, S. G., McTernan, J. K., Gilchrist, B. E., Bell, I. C., Voronka, N. R., and Hoyt, R. P., "Electrodynamic Tethers for Energy Harvesting and Propulsion on Space Platforms," AIAA SPACE 2010 Conference and Exposition, No. AIAA-2010-884, Aug. 2010.
41. Atchison, J. and Peck, M., "Length Scaling in Spacecraft Dynamics," *Journal of Guidance, Control, and Dynamics*, Vol. 34, No. 1, pp. 231–246, 2011.
42. Kubo-oka, T. and Sengoku, A., "Solar Radiation Pressure Model for the Relay Satellite of SELENE," *Earth Planets Space*, Vol. 51, pp. 979–986, September 1999.
43. Voronka, N., Hoyt, R.P., Gilchrist, B. E., and Fuhrhop, K., "An Architecture of Modular Spacecraft with Integrated Structural Electrodynamic Propulsion (ISEP)," NIAC 7 the Annual Meeting, Tucson, AZ, 18 October 2006.